Scanning Microscopy

Volume 7 | Number 4 Article 4

12-29-1993

# Caesium on Si(100) Studied by Biassed Secondary Electron Microscopy

M. Azim
*University of Sussex*

C. J. Harland
*University of Sussex*

T. J. Martin
*University of Sussex*

R. H. Milne
*University of Sussex*

J. A. Venables
*University of Sussex*

Scanning Microscopy, Vol. 7, No. 4, 1993 (Pages 1153-1160) 0891-7035/93$5.00+.00
Scanning Microscopy International, Chicago (AMF O'Hare), IL 60666 USA

# CAESIUM ON Si(100) STUDIED BY BIASSED SECONDARY ELECTRON MICROSCOPY

M. Azim[1], C.J. Harland[1], T.J. Martin[1], R.H. Milne[1,*] and J.A. Venables[1,2]

[1]School of Mathematical and Physical Sciences, University of Sussex, Brighton BN1 9QH, UK.
[2]Department of Physics and Astronomy, Arizona State University, Tempe, Arizona, AZ 85287, USA.

(Received for publication September 30, 1993, and in revised form December 29, 1993)

## Abstract

An ultra-high vacuum scanning electron microscope (UHV-SEM) has been used to study sub-monolayers of Cs on Si(100) surface. Cs adsorption on the surface causes a considerable change in the work function. Coverages below 1/2 monolayer (ML) have been estimated by correlating the work function changes with the secondary electron (SE) signal. It has been found that this signal is sensitive down to ~ 0.005 ML when the sample is biassed to a few hundred volts.

Electron trajectories from a biassed sample have been simulated for electrons originating from different areas with different work functions across the sample. This indicates that variations in coverage can be determined by secondary electron imaging provided these coverages are less than 1/2 ML.

The diffusion of Cs (< 1/2 ML) above room temperature has been studied using the biassed-SE imaging technique. Observed diffusion profiles have unusual features including two linear regions. These can be explained by a model which contains two competing adsorption sites, and includes blocking of the diffusion paths by other Cs atoms.

**Key Words**: Adsorption, alkali metals, caesium, diffusion, microscopy, secondary electrons, semiconductors, silicon, surfaces, work function.

*Address for correspondence:
R.H. Milne,
School of Mathematical and Physical Sciences,
University of Sussex,
Brighton BN1 9QH, U.K.
Telephone number: 0273 606755 ext. 3078
FAX number: 0273 678097

## Introduction

Understanding alkali metal (AM) adsorption on semiconductor surfaces is very important for several aspects of surface science. The structure and bond strengths at different coverages indicate how metal/semiconductor interfaces are formed. As the AM coverage increases the work function (WF) decreases dramatically [12] and co-adsorption with oxygen can produce negative electron affinity (NEA) surfaces [9] (where the WF is reduced so much that the vacuum level at the surface of the semiconductor is lower than the bulk position of the bottom of the conduction band). This has considerable practical importance as NEA surfaces can act as highly efficient electron emitters. Alkali metals are also known to act as catalysts to enhance oxidation of the semiconductor substrate [10, 11, 14, 16].

In this paper we look at the Cs/Si(100) system. The silicon retains its clean surface 2x1 reconstruction as Cs increases to saturation [15]. The exact saturation level has not unambiguously been settled but recent results suggest that a full monolayer (ML) can be deposited onto the surface [1, 13, 17]. It has been suggested that the pedestal sites are the preferred adsorption sites at coverages up to 1/2 ML, beyond which sites between the dimer rows are occupied, until the monolayer coverage is reached. The WF decreases with Cs coverage until, at approximately 1/2 ML coverage, a WF minimum is reached and then increases to a constant value at saturation Cs coverage. In this paper, we assume that the WF minimum is at 1/2 ML and saturation corresponds to a full ML. Work function changes are used to quantify local Cs concentrations on the surface; both the initial deposition and the distribution after heating the sample, which monitors the desorption and diffusion.

We have used an ultra-high vacuum scanning electron microscope (UHV-SEM) to monitor the secondary electron (SE) signal produced by a focused 30 kV electron beam and thereby observed and studied very thin adsorbed layers. As a consequence of the drop in WF upon AM adsorption, a substantial increase in secondary electron yield occurs. However, if the adsorbate is in the form of patches on the substrate, the WF changes across the sample generate electric fields, in the

vacuum, around the patch and these "patch fields" can reduce the number of SEs reaching the detector. The extent of the patch fields into the vacuum is comparable to the width of the patch and so the effect of these fields can be reduced by applying a potential gradient above the sample. This is most easily done by biasing the sample negative and this is the basis of the technique of biassed secondary electron imaging (b-SEI).

The b-SEI technique was previously utilized to study the diffusion of Cs on polycrystalline tungsten [8]. In that case, a cylindrical mirror analyzer was used to measure the WF changes directly [2, 8]. The changes in SE signal were analyzed [4] by calculating the trajectories of SEs leaving a biassed sample at various positions, energies, and angles. The surface was modelled as two semi-infinite regions, one being clean tungsten and the other W covered with a monolayer Cs. Further b-SEI studies on a variety of adsorbate-substrate systems have shown the general usefulness of the technique [3, 4, 6, 7]. In the case of Ag on Si(111) and (100) the sensitivity was reported to be 0.1 ML with a sample bias voltage $V_b$ = -500 V.

In the present study we have been able to observe sub-monolayers of Cs on the Si(100) 2x1 surface, and a sensitivity of 0.5% of a monolayer ( ~ 3.4 x $10^{12}$ atoms $cm^{-2}$) has been obtained. Biassed secondary electron linescans give important information about the Cs adlayers regarding adsorption and expansion of patches as the sample is heated. The simulation of electron trajectories has been extended to model the changes of work function present across the sample as it is heated and the results are discussed in sections on **Experimental Observations**, and **Discussion and Conclusions**. We briefly describe the unusual diffusion profiles obtained from this system (for coverages below 1/2 ML) and show that most of the features can be explained by assuming two competing adsorption sites and blocking of diffusion pathways.

## Experimental Techniques

The microscope used for the present work has been previously described [5, 18, 19]. The electron beam from a field emission gun (FEG) is used for SEM observations. Secondary electrons are collected by an Everhart-Thornley detector. A cylindrical mirror analyzer (CMA) can be racked into position for Auger electron spectroscopy (AES) and scanning Auger microscopy. Crystallographic orientation and structural properties of the sample can be studied by reflection high energy electron diffraction (RHEED) using a fluorescent screen on top of the chamber, by tilting the sample about a horizontal axis.

For the present work, Si samples were cut to a size of 22 mm x 5 mm (p-type, $\rho$ = 7-13 Ω-cm) from a wafer covered with a CVD (chemical vapor deposited)-epilayer of 4 $\mu$m thickness. The sample was pressed between tantalum clips and cleaned by passing a direct current for flash heating up to 1150°C at a base pressure of 1 x $10^{-10}$ torr. The temperature was measured by an optical pyrometer. Lower temperatures were measured by an infrared pyrometer which was calibrated to a standard thermocouple. Si(100) reconstructs into the 2x1 structure which was observed by RHEED. Cs was deposited from a SAES getter dispenser after the sample was found to be clean to the detection limits of AES. Cs was deposited through a mask with holes in it producing Cs patches of various sizes on the sample (at the deposition rate of 0.1 ML/min). The mask was flipped back from in front of the sample after deposition.

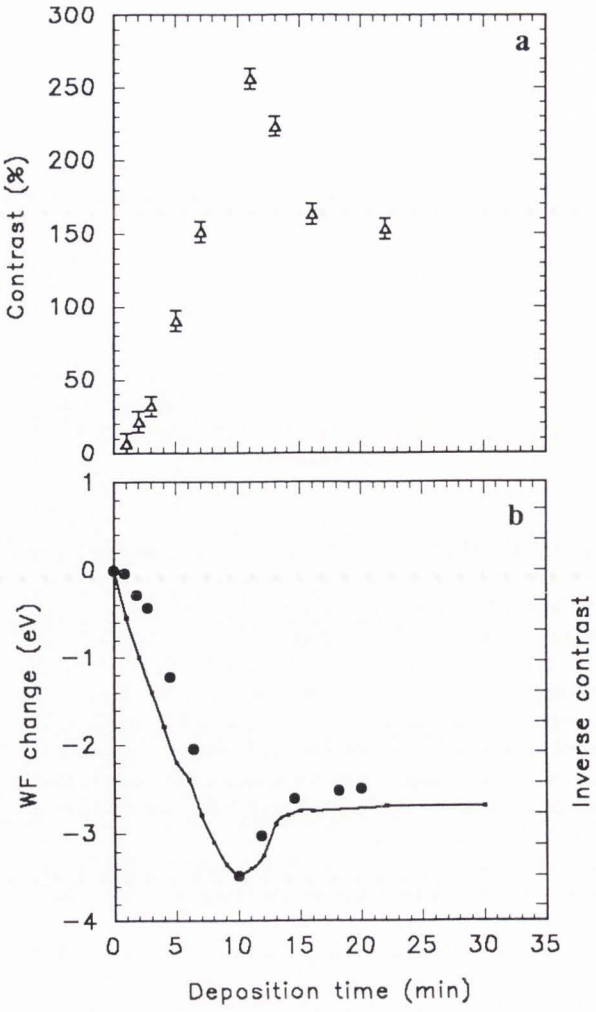


**Figure 1.** **a**: b-SE contrast with deposition time at constant deposition rate. **b**: Comparison of the contrast and work function changes with deposition time (full line shows reconstructed WF change and dots show the contrast inverted and rescaled).

## Experimental Observations

### Cs coverage estimates

Patches of Cs were formed by depositing Cs through the mask as described above. 100 $\mu$m x 100 $\mu$m

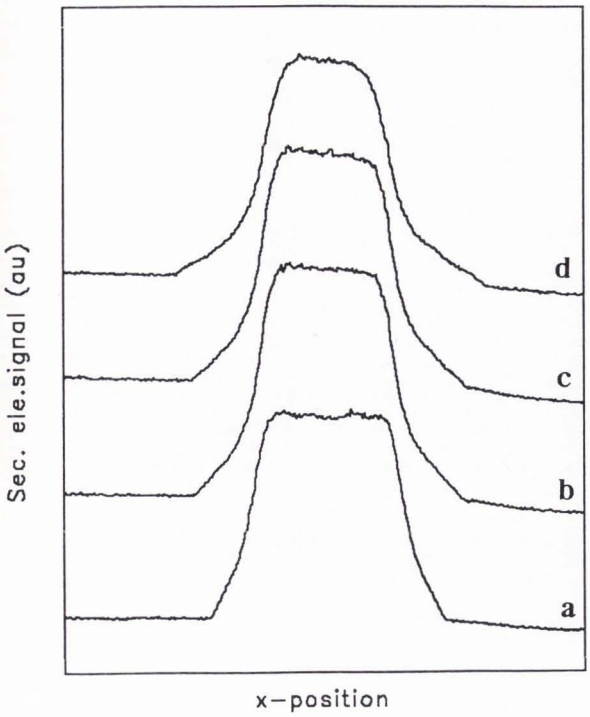


**Figure 2**. Biassed secondary electron linscans across the patch at 0.23 ML coverage: **a**: after room temperature deposition; and **b**, **c**, and **d**: after 5, 10, and 20 minutes heating, respectively, at 60°C.

patches were used in the present studies. A large decrease in the work function of the substrate caused by deposited sub-monolayers {$\Delta\phi$ = -3.4 eV at 1/2 ML of Cs on Si(100) surface} considerably increases the secondary electron yield. This produces SE contrast between the clean Si and the Cs patches with b-SEI. In the work described here, the sample was always biassed at $V_b$ = -600 V. No contrast could be observed with conventional SEM at any coverage.

Calibration of Cs coverage was achieved by measuring the contrast between the Si substrate and the Cs patches for various deposition times. Linescans across a patch were taken and the contrast determined by C = {(averaged signal at center of the patch) minus (the signal from the Si) divided by (the Si signal)}. Figure 1a shows the b-SE contrast as a function of deposition time with a fixed source temperature. The contrast increases with increasing deposition time, approaching the maximum of ~ 250% and then decreases to a constant value. This has been compared with the work function changes in Figure 1b. This WF curve has been reconstructed from the published data [12] and our contrast values have been inverted and rescaled. The general pattern of the contrast is similar to the WF changes. The Cs coverage is now estimated by assuming that the maximum contrast corresponds to the WF minimum and that this corresponds to 1/2 ML of Cs. From this procedure, it is estimated that Cs patches with a coverage of ~ 0.005

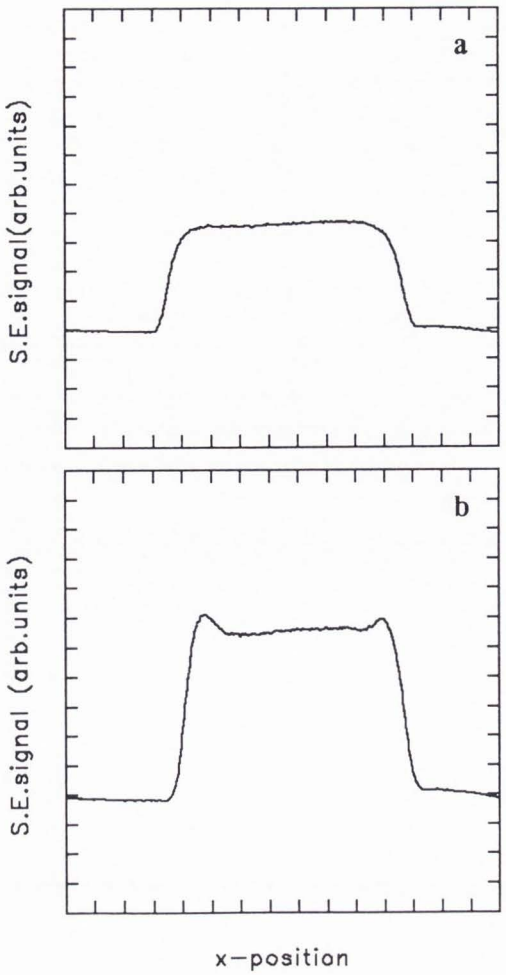


**Figure 3**. Biassed SE linescans across a patch. **a**: At saturation coverage. **b**: After flashing at 150°C for 5 seconds.

ML can be detected. The high sensitivity of the b-SEI is obvious from Figure 2a which is a linescan across a Cs patch with a coverage of 0.23 ML in the center. The signal at the edge of this patch clearly shows contrast at ~ 1/50th of the central signal. This indicates that good relative coverages can be determined but absolute coverages probably have an error of about 5%.

**Contrast across patches at high coverage**

When ~ 1 ML of Cs is deposited through the mask, quite sharp Cs-Si boundaries around the patches are observed. Assuming a concentration gradient at the edge, the WF changes from a certain intensity, corresponding to 1 ML, to that corresponding to zero Cs concentration with the WF minimum somewhere between saturation and zero concentration. It might therefore be reasonable to expect an area close to the edge of a patch to appear brighter than the central region corresponding to the lowest WF at 1/2 ML concentration. SE linescans across a patch would then give two peaks at positions close to the edges. These were not observed, as can be

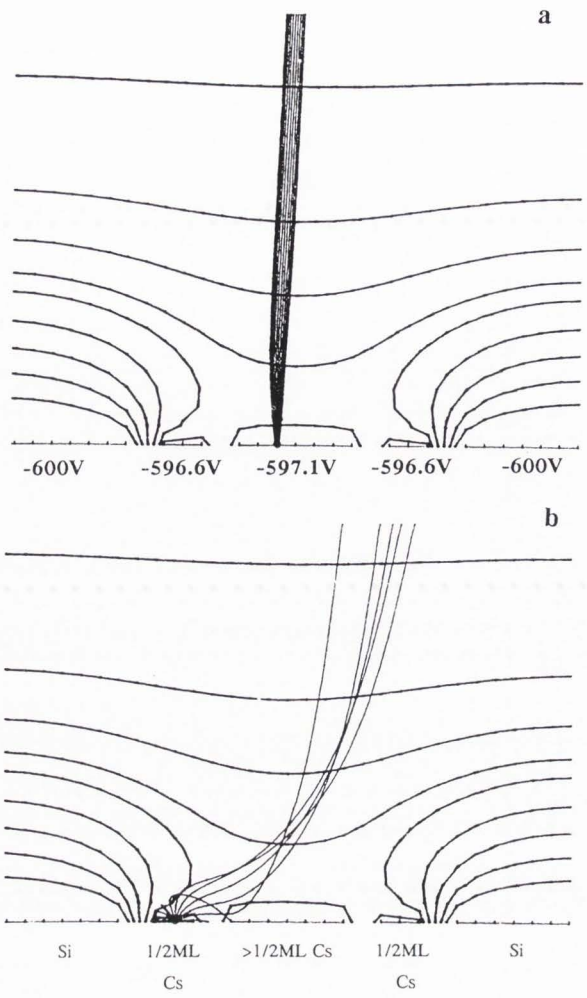


**Figure 4**. Simulated electron trajectories from a Cs patch with 1 ML coverage in the central region for, **a**: electrons originating with energy 0.001 eV from the region of saturation coverage; all of them reach the detector; and, **b**: electrons originating with energy 0.51 eV from 1/2 ML region; about half of them can reach the detector. The angular range of the electrons is 15°-165° and the field applied is -400 V/cm.

---

seen from Figure 3a which is a linescan across such a patch at saturation Cs concentration. The expected peaks in the linescans were, however, observed after the sample was flashed for ~ 5 seconds to about ~ 150°C. This is clear from Figure 3b which is the linescan, after flashing, across the same position on the patch as in Figure 3a. Comparison of Figure 3b with Figure 3a shows that the contrast of the central region has increased from ~ 133% for saturation to about ~ 235%.

We can explain these observations by assuming that there is a subsidiary patch field around the WF minimum. The extent of a patch field into the vacuum is similar to the lateral dimensions of the corresponding area on the surface. If the 1/2 ML region is small, then the associated patch field does not extend far above the

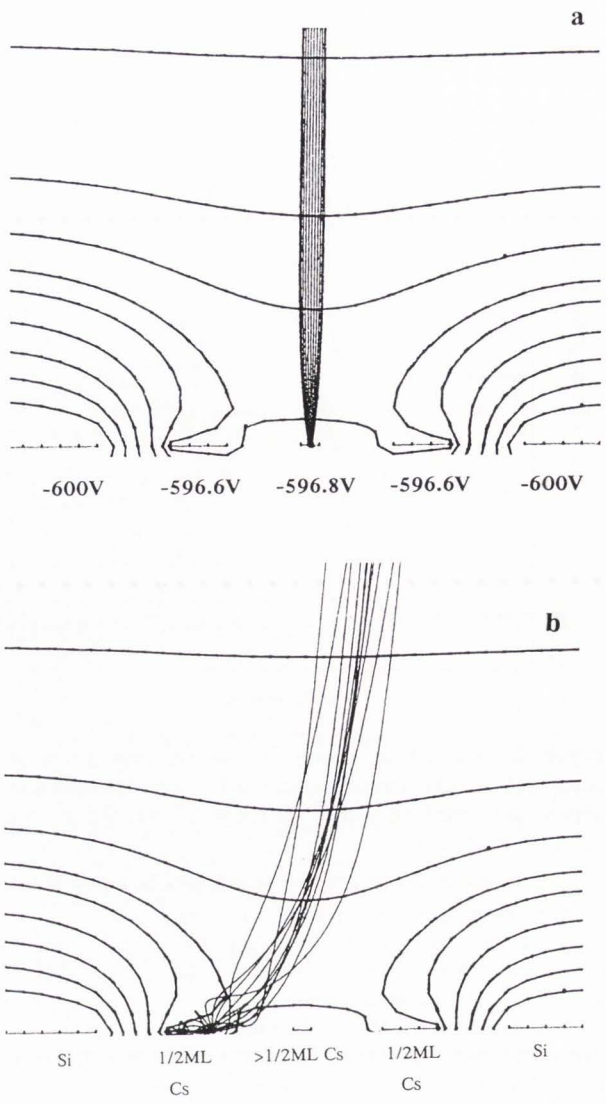


**Figure 5**. Simulated electron trajectories for, **a**: electrons originating with 0.001 eV energy from the region above 1/2 ML; and, **b**: electrons originating with energy 0.16 eV from 1/2 ML region. The 1/2 ML region has been expanded (for explanation see text).

---

surface and so the bias field has very little effect. After flashing we assume that the area of 1/2 ML coverage expands as desorption occurs in the central region. The increase of the 1/2 ML area coupled with a smaller change in WF between this region and the center (where the concentration is estimated to be ~ 0.6 ML) allows most of the extra electrons to escape; these give the bright edge in the b-SE linescan.

To test our ideas regarding these observations we have extended the previous work done for the electron trajectories originating from a surface with a sharp change in WF [8] to one with various changes of WF across the sample. Potential contours and the trajectories of electrons with various energies and angles have

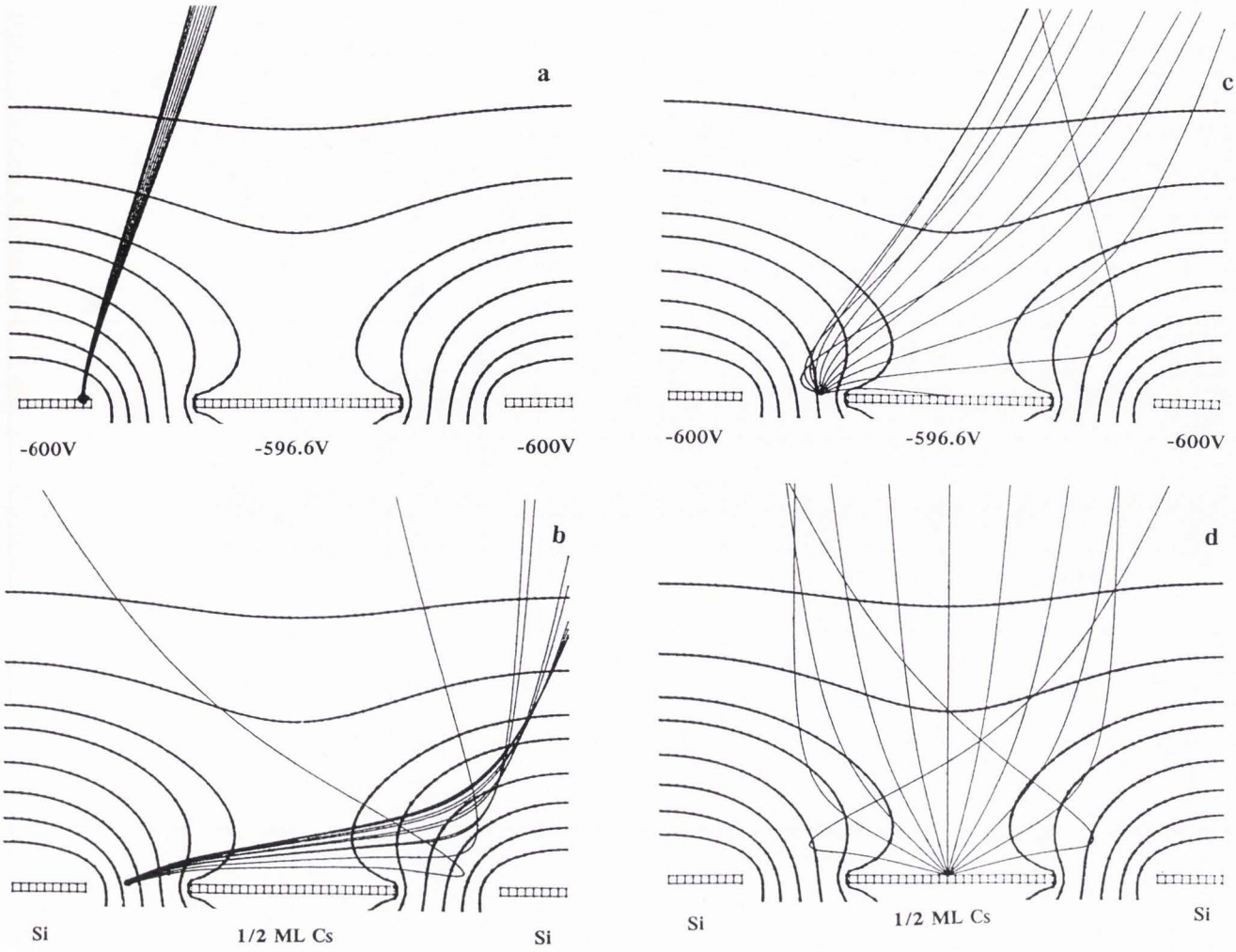


**Figure 6**. Electron trajectories of, **a**: 0.001 eV electrons originating from the substrate; **b**: 0.01 eV electrons originating from a position where the WF is 1.7 eV below; **c**: 0.5 eV electrons originating from a position where the WF is 2.6 eV below; and, **d**: 1.0 eV electrons from a position where the WF is 3.4 eV below that of the Si substrate.

---

been simulated by using 'SIMION 4.0'. This is an electrostatic lens analysis and design program in which a lens is defined as a 2-dimensional array of points forming a grid. Each grid point is referred to as either an electrode or non-electrode. The electrode points can be combined together to define the shape of an electrode, in this case with planar non-symmetric geometry. Once the geometry is set, different voltages can be applied to the individual electrodes. Potentials at non-electrode grid points are calculated using a dynamically self-adjusting over-relaxation method. The numerical integration of trajectories can then be carried out.

The simulation work was done for two cases corresponding to Figures 3a and 3b. We applied a high field of -400 V/cm and assigned different potentials to individual electrodes according to the WF variations. Electron trajectories for electrons with different energies are shown in Figures 4 and 5. It is seen from Figure 4 that all the electrons originating with 0.001 eV from the central area covered with the full monolayer can reach the detector, whereas about half of the electrons with energy 0.51 eV (i.e., greater than the WF difference) from the area with 1/2 ML are unable to overcome the subsidiary patch fields and hence cannot reach the detector. This means that we cannot see the bright edges in the image, or peaks in the b-SE linescans.

For the other case the 1/2 ML areas were broadened in size and the higher coverage area at the center was reduced producing a WF difference of 0.2 eV. The simulation results (see Fig. 5) show that the electrons originating from the inner edge of the 1/2 ML area with energies less than 0.16 eV could escape the fields and can reach the detector. Therefore, a higher yield of electrons from this region is detected making the region brighter and giving the peaks seen in the b-SE linescans.

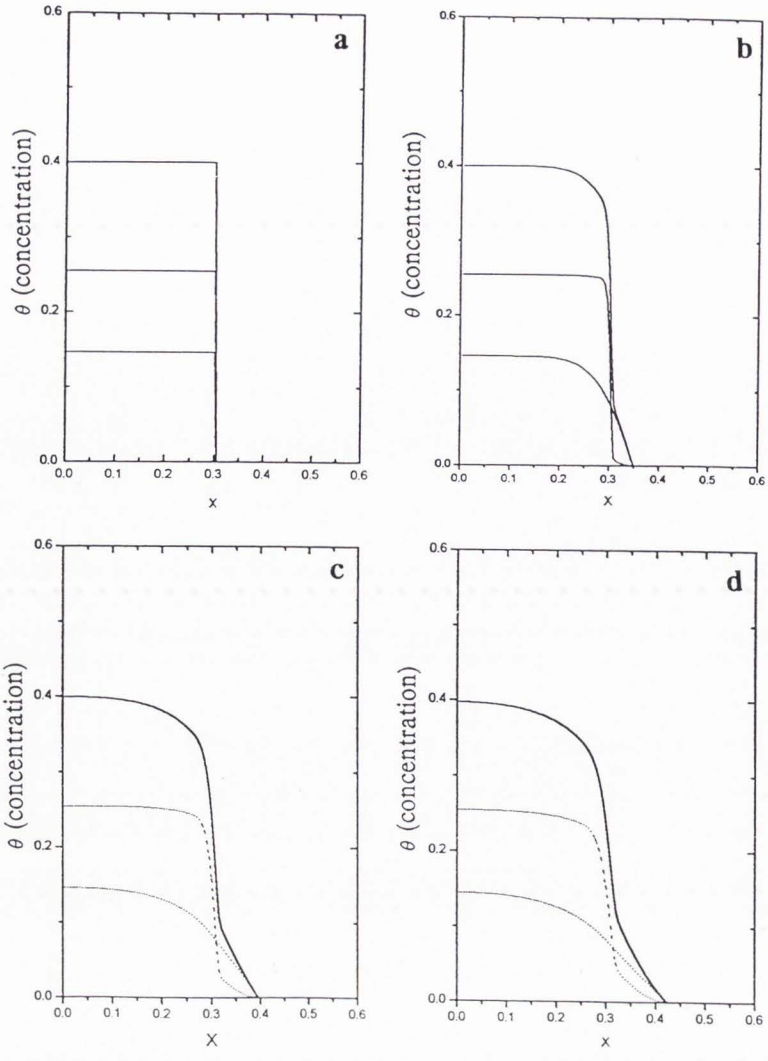


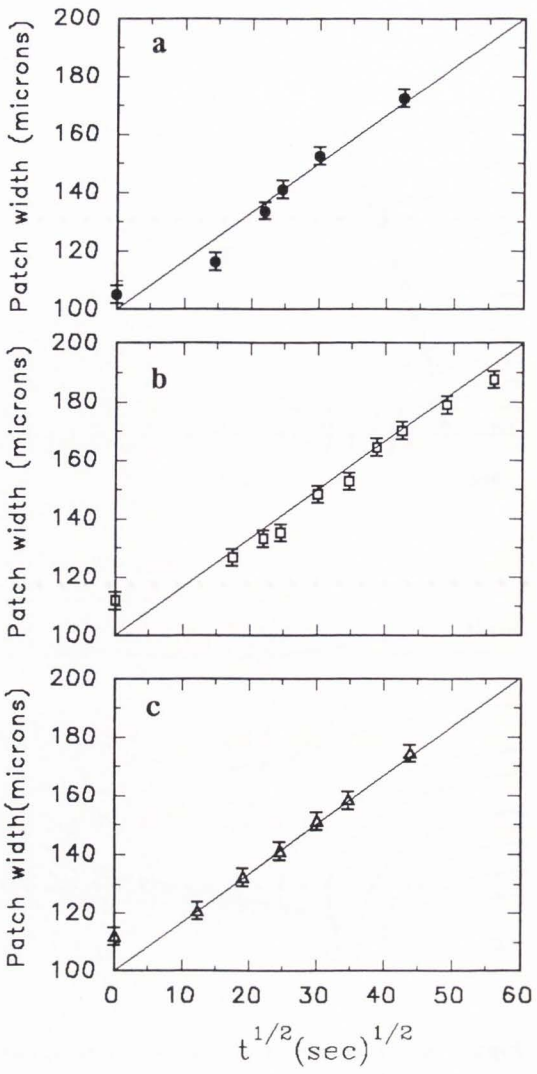


**Figure 7 (at left).** Patch width plotted against $t^{1/2}$ for three coverages, **a**: 0.13 ML; **b**: 0.23 ML; and **c**: 0.32 ML when heated at 60°C. The linear increase of patch width with $t^{1/2}$ is independent of coverage and has equal values.

**Figure 8 (at right).** Time evolution of diffusion profiles using the equations (described in the text) with fitting parameters $D_1 = 0.02\ cm^2s^{-1}$; $D_2 = 2.0\ cm^2s^{-1}$; $\tau_{12} = 6000$ and $\tau_{21} = 500$.

---

The expansion of the 1/2 ML region during flashing is due to the adsorption sites occupied by the Cs atoms at different coverages. For up to 1/2 ML coverages, most of the Cs atoms will be strongly bonded at the pedestal sites. For greater coverages, the Cs atoms occupy sites between the dimer rows and are less strongly bonded. Therefore, flashing the sample briefly at ~ 150°C tends to reduce the coverage in the center and the 1/2 ML region extends inwards. Further experiments on desorption from saturated Cs layers have helped to confirm the stability of the 1/2 ML coverage. It is also fairly easy to remove the second half monolayer by electron beam irradiation. Bright lines or spots can be created in the middle of a 1 ML patch by electron irradiation for a few minutes. These bright areas are attributed to regions of 1/2 ML coverage which are then fairly stable under the beam.

**Annealing after room temperature deposition, low coverage studies**

For patches less than 1/2 ML coverage interpretation of the images and linescans is easier. Very little electron beam desorption is observed and the WF profiles across the surface are much simpler. Given a high bias field of -400 V/cm most of the secondary electrons emitted can be detected (Fig. 6) and so the signal intensity can be translated into concentration profiles, particularly around the diffused region. This allows the diffusion of Cs across the surface to be monitored.

Surface diffusion of the Cs patches was studied by heating the sample after the depositions were carried out at room temperature. Separate experiments were performed at different coverages and various temperatures. The temperature range over which these experiments were per-

formed was limited to below 100°C since desorption of the deposited Cs has been observed at high temperatures. The results described here are for the diffusion of Cs at ~ 60°C, as at this temperature, desorption appears to be fairly small. Figures 2b-2d show some b-SE linescans across a patch during heating for periods (t) of 5, 10 and 20 minutes. Results are shown in Figure 7 for the variation of patch width with time for three different coverages (0.13, 0.23 and 0.32 ML). The results presented in Figure 7 for diffusion of Cs on Si(100) show that the patch width increases linearly with $t^{1/2}$. Using the general equation relating the diffusion lengths ($l_d$) to time (t), i.e.,

$$\langle l_d^2 \rangle = 2Dt$$

the effective diffusion coefficient, D, for the atoms can be estimated.

More detailed discussions of the Cs diffusion will subsequently be presented but some interesting results are obviously apparent (Figure 2). Although the edge of the patch diffuses with the expected $t^{1/2}$ dependence the actual profiles do not have the 'classical' error function shape. The profiles seem to have two distinct components, both are fairly linear initially and the outer part retains this linearity throughout the experiment.

At room temperature, the saturation coverage of Cs on Si(100) is 1 ML indicating that Cs sitting on Cs is not a favorable configuration. This means that as diffusion occurs, Cs atoms do not jump over each other and so some Cs atoms can block the diffusion path for other Cs atoms. This can be modelled by letting the diffusion coefficient depend on $\theta$ (1 - $\theta$) where $\theta$ represents the fractional coverage of a particular set of sites. That is, the diffusion depends both on the number of atoms and the number of empty sites. A diffusion equation of the form:

$$\frac{\partial \theta}{\partial t} = \frac{\partial}{\partial x}\left(D(\theta)\frac{\partial \theta}{\partial x}\right)$$

with x being the distance from original interface and $D(\theta) = D_1 (\theta - \theta^2)$ has a solution

$$\theta = \frac{x}{2\sqrt{D_1 t}} + \frac{1}{2}$$

where $D_1 = 2D$. Assuming a sharp interface initially, this solution gives a straight line diffusion profile with the edge moving with a $t^{1/2}$ dependence.

In the results shown in Figure 2 there seems to be two distinct components. We can model this by two coupled differential equations in which atoms can diffuse along two different types of pathways. Without making any assumptions as to the particular sites or phases involved, we can assume that the different sites have different binding energies and different diffusion coefficients. However, we also assume that the Cs atoms can interchange between the two sites or phases. This is characterized by a particular time between jumps: $\tau$. This results in coupled equations of the form:

$$\frac{\partial \theta_1}{\partial t} = \frac{\theta_2(1 - \theta_1)}{\tau_{21}} - \frac{\theta_1(1 - \theta_2)}{\tau_{12}} + D_1 \frac{\partial}{\partial x}\left(\theta_1(1 - \theta_1)\frac{\partial \theta_1}{\partial x}\right)$$

and

$$\frac{\partial \theta_2}{\partial t} = \frac{\theta_1(1 - \theta_2)}{\tau_{12}} - \frac{\theta_2(1 - \theta_1)}{\tau_{21}} + D_2 \frac{\partial}{\partial x}\left(\theta_2(1 - \theta_2)\frac{\partial \theta_2}{\partial x}\right)$$

where $\theta_1$, $\theta_2$ are the coverages of the two sites, $\tau_{12}$ and $\tau_{21}$ are the jump times from site 1 to site 2 and from site 2 to site 1, respectively, and $D_1$, $D_2$ are the diffusion coefficients for atoms in site 1 and site 2. Solving these equations numerically for various values of $\tau$ and D can reproduce several of the features shown by the experimental results of Figure 2.

In these calculations, no attempt has been made to scale the results; instead we have tried to reproduce the general pattern of diffusion (Figure 8). The main points are that early on in the diffusion profiles, both components are linear, and as time progresses, the lower coverage 'tongue' remains linear while the higher coverage part starts to become more curved. These general features are in accord with the experimental profiles and, of course, the patch width expands as $t^{1/2}$.

## Discussion and Conclusions

Biassed secondary electron imaging is a useful technique for examining the general behavior of sub-monolayer coverages of adsorbates, especially in systems such as Cs/Si where the work function changes are pronounced. Coverage determination down to ~ 0.005 ML can be achieved in a few minutes and this is generally better than most scanning Auger systems due, primarily, to the higher signal. The speed of acquisition is particularly important for systems where electron beam effects and contamination problems restrict the time available. However, interpretation of results requires care. Small areas with lower WF might give no contrast if the bias field is not strong enough and modelling of secondary electron trajectories is a sensible precaution. Our trajectory simulations presented here are qualitative; more detailed calculations including the secondary electron energy and angular distributions should also be carried out. Because of possible difficulties in the interpretation of high coverage cases, our analysis of Cs diffusion has been restricted to fairly low coverages, where most of the secondary electrons generated (particularly near the edge of the patches) are able to overcome the patch fields.

Although more detailed analysis is required, the results for Cs on Si(100) have already provided some interesting information. Thermal and electron beam assisted desorption both support the general adsorption model of two sites being occupied sequentially. Low coverage diffusion gives unusual linear concentration profiles that can be explained by the blocking of the diffusion paths by other Cs atoms. The idea that the two sets of adsorption sites required to model the complete diffusion profile are the sequential rows of pedestal and sites between the dimers is

appealing, but may well need elaboration. First, atoms on sites between the dimers desorb easily, particularly under the electron beam and second, the bonding energies of the two sites required to produce the correct profile (not discussed here) are probably too close. A good description of these two bonding sites is still required and probably needs adsorbate-adsorbate interactions (and hence more surface structure information) to be included.

**Acknowledgements**

We are grateful for SERC funding and one of us (MA) thanks the Government of the Islamic Republic of Pakistan for financial support.

**References**

1. Abukawa T, Kono S (1988) Photoelectron diffraction studies of Si(100) 2x1-K surface: existence of a potassium double layer. Phys. Rev. **B 37**, 9097-9099.

2. Akhter P, Venables JA (1981) SEM observations of caesium monolayers on polycrystalline tungsten. Surf. Sci. **103**, 301-314.

3. Drucker J, Krishnamurthy M, Hembree G (1991) Biassed secondary electron imaging of monoatomic steps on vicinal Si(100) in a UHV-STEM. Ultramicros. **35**, 323-328.

4. Futamoto M, Hanbucken M, Harland CJ, Jones GW, Venables JA (1985) Visualization of sub-monolayers and surface topography by biassed secondary electron imaging: Application to Ag layers on Si and W surfaces. Surf. Sci. **150**, 430-450.

5. Harland CJ, Venables JA (1985) Digital data acquisition, display and analysis of signals from surfaces. Ultramicrosc. **17**, 9-19.

6. Harland CJ, Jones GW, Doust T, Venables JA (1987) Scanning electron microscopic observations of monolayer deposits using biassed secondary electron and specimen current imaging. Scanning Microscopy Suppl. **1**, 109-114.

7. Hembree GG, Crozier PA, Drucker JS, Krishnamurthy M, Venables JA, Cowley JM (1989) Biassed secondary electron imaging in a UHV-STEM. Ultramicrosc. **31**, 111-115.

8. Janssen AP, Akhter P, Harland CJ, Venables JA (1980) High spatial resolution surface potential measurements using secondary electrons. Surf. Sci. **93**, 453-470.

9. Martinelli RU (1970) Infrared photoemission from silicon. App. Phys. Letts. **16**, 261-262.

10. Michel EG, Ortega JE, Oellig EM, Asensio MC, Ferron J, Miranda R (1988) Early stages of the alkali-metal promoted oxidation of silicon. Phys. Rev. **B 38**, 13399-13406.

11. Ortega JE, Oellig EM, Ferron J, Miranda R (1987) Cs and O adsorption on Si(100)2x1: A model system for promoted oxidation of semiconductors. Phys. Rev. **B 36**, 6213-6216.

12. Papageorgopoulos CA, Kamaratos M (1989) Adsorption of Cs and its effects on the oxidation of the $Ar^+$ sputtered Si(100) 2x1 substrate. Surf. Sci. **221**, 263-276.

13. Smith AJ, Graham WR, Plummer EW (1991) Coverage measurements of the Si(100) 2x1:Cs and Si(100) 2x1:K surfaces: resolution of structural models. Surf. Sci. Letts. **243**, L37-L40.

14. Soukiassian P, Gentle TM, Bakshi MH, Hurych Z (1986) $SiO_2$-Si interface formation by catalytic oxidation using alkali metals and removal of the catalyst species. J. Appl. Phys. **60**, 4339-4341.

15. Soukiassian P, Kim ST, Hurych Z, Rubby JA (1992) Structural Properties of Alkali metal/Si(100) 2x1 interfaces investigated by PEXAFS and STM. Appl. Surf. Sci. **56-58**, 394-401.

16. Starnberg HI, Soukiassian P, Bakshi MH, Hurych Z (1988) Thermal growth of $SiO_2$-Si interface on Si(111) 7x7 surface modified by caesium. Phys. Rev. **B 37**, 1315-1319.

17. Urano T, Sakaue K, Nagano K, Hongo S, Kanaji T (1991) Adsorption structure of K on Si(100) at various coverages. J. Crystal Growth **115**, 411-417.

18. Venables JA, Janssen AP, Akhter P, Derrien J, Harland CJ (1980) Surface studies in a UHV field emission gun electron microscope. J.Microsc. **118**, 351-365.

19. Venables JA, Spiller GD, Fathers DJ, Harland CJ, Hanbucken M (1983) UHV SEM studies of surface processes - Recent studies. Ultramicrosc. **11**, 149-155.

**Discussion with Reviewers**

**K. Murata**: Why is the work function change maximum at 0.5 ML?
**Authors**: This is still a matter for debate but involves changes in the electronic structure of the adsorbate including depolarization and metallization.

**K. Murata**: Is there a optimum bias voltage to give the maximum contrast?
**Authors**: We do find an optimum bias and run our experiments close to this voltage of -600 V. The transport of electrons inside the microscope chamber is quite complex and the collection efficiency depends on the sample position and bias.

**K. Murata**: You have used 30 keV electron beam, the Bethe range of which is larger than 10 $\mu$m. Isn't it necessary to take into consideration the spatial distribution of secondary electrons produced by backscattered electrons when you study the diffusion length of Cs?
**Authors**: The production of secondary electrons by backscattering is important. In general, for 30 keV electrons incident on Si a lot of these secondaries are emitted within $\sim$ 4 $\mu$m of beam and do degrade the resolution by this amount. In our geometry, the beam is incident at $\sim$ 30° to the surface and the forward scattering is parallel to the patch edge and perpendicular to the direction of diffusion. This helps to reduce the degradation of the resolution to $\sim$ 1-2 $\mu$m maximum.

**K. Murata**: I presume that secondary electrons excited by backscattered electrons at the chamber wall are also detected. If you can remove these electrons with some device, is there any possibility to improve the b-SE contrast?
**Authors**: Preliminary calculations of the expected contrast with change of WF give good agreement with our results if a background component is included. This suggests that the contrast can be improved in the future. Energy analysis can be used, as in ref. [4], but at the cost of reduced signal level.